



Aerodynamic rotor design for a 25 MW offshore downwind turbine

Michael Jeong^{a,*}, Eric Loth^a, Chris Qin^b, Michael Selig^c, Nick Johnson^d

^a Department of Mechanical and Aerospace Engineering, University of Virginia, USA

^b School of Engineering and Computer Science, Washington State University, USA

^c Department of Aerospace Engineering, University of Illinois at Urbana-Champaign, USA

^d Sandia National Laboratories, USA

HIGHLIGHTS

- Three 25 MW downwind offshore rotors with varying chord and twist were designed.
- Blade geometry and rotor swept area were considered for maximizing power production.
- Empirical correlations were found to estimate flatback airfoil characteristics.
- A design space was created to validate prescribed lift coefficient distributions.
- Simulations were performed to predict power production and optimize rotor mass.

ARTICLE INFO

Keywords:

Wind turbine rotor design
Wind turbine aerodynamics
Extreme-scale wind turbines
Wind turbine design parameters
Offshore wind energy
Downwind rotors

ABSTRACT

Continuously increasing offshore wind turbine scales require rotor designs that maximize power and performance. Downwind rotors offer advantages in lower mass due to reduced potential for tower strike, and is especially true at large scales, e.g., for a 25 MW turbine. In this study, three 25 MW downwind rotors, each with different prescribed lift coefficient distributions were designed (chord, geometry, and twist) and compared to maximize power production at unprecedented scales and Reynolds numbers, including a new approach to optimize rotor tilt and coning based on aeroelastic effects. To achieve this objective the design process was focused on achieving high power coefficients, while maximizing swept area and minimizing blade mass. Maximizing swept area was achieved by prescribing pre-cone and shaft tilt angles to ensure the aeroelastic orientation when the blades point upwards was nearly vertical at nearly rated conditions. Maximizing the power coefficient was achieved by prescribing axial induction factor and lift coefficient distributions which were then used as inputs for an inverse rotor design tool. The resulting rotors were then simulated to compare performance and subsequently optimized for minimum rotor mass. To achieve these goals, a high Reynolds number design space was developed using computational predictions as well as new empirical correlations for flatback airfoil drag and maximum lift. Within this design space, three rotors of small, medium and large chords were considered for clean airfoil conditions (effects of premature transition were also considered but did not significantly modify the design space). The results indicated that the medium chord design provided the best performance, producing the highest power in Region 2 from simulations while resulting in the lowest rotor mass, both of which support minimum LCOE. The methodology developed herein can be used for the design of other extreme-scale (upwind and downwind) turbines.

1. Introduction

As the need for energy increases globally, renewable energy has become the fastest-growing segment of the energy sector, providing cleaner sources of energy that will have less impact on growing

environmental problems. Wind energy is anticipated to become one of primary renewable energy sources. In 2008, the Department of Energy set a target for wind energy to provide 20% of U.S. energy by 2030 [1]. More recently in 2021, the Biden Administration announced a national offshore wind target of 30 GW by 2030 [2]. Currently, the largest commercial wind turbines are rated at 14 MW [3], but trends are going

* Corresponding author.

E-mail address: mwj2pf@virginia.edu (M. Jeong).

<https://doi.org/10.1016/j.apenergy.2023.122035>

Received 15 April 2022; Received in revised form 23 July 2023; Accepted 27 September 2023

0306-2619/© 2023 Published by Elsevier Ltd.

Nomenclature			
<i>Roman letters</i>		θ	Twist angle
a	Axial induction factor	λ	Tip-speed ratio
c	Chord	Ψ	Azimuthal angle
C	Coefficient	<i>Subscripts</i>	
m	Mass	<i>blade</i>	Blade value
P	Aerodynamic power	d	Drag value
r	Local blade radius	l	Local lift value
R	Blade radius (root to tip)	<i>lower</i>	Lower limit
t	Thickness	<i>max</i>	Maximum value
T	Aerodynamic thrust	P	Power value
U	Wind speed	<i>rated</i>	Rated value
y	Deflection	<i>rigid</i>	Rigid case
<i>Greek letters</i>		T	Thrust value
α	Angle of attack	TE	Trailing edge value
β	Blade pitch angle	<i>tip</i>	Blade tip value
		<i>upper</i>	Upper limit
		0	Value at $\alpha = 0^\circ$

toward continuously increasing scales. Extreme-scale offshore wind turbines present an opportunity for even more energy production as offshore wind is more abundant than land-based wind. Increasing turbine sizes to extreme-scales also allows for more energy capture while having less leveled cost of energy (LCOE) [1,4]. Downwind rotors offer advantages in lower mass due to reduce potential for tower strike, especially at the extreme-scales used in this study [5]. Offshore wind energy presents valuable opportunities to increase the amount of renewable energy in the grid with very suitable environments to implement in areas like the United States and Europe [6,7]. However, these extreme-scales also pose certain structural limitations in blade loads and deflections due to longer blades and higher offshore wind speeds and turbulence. Using conventional rotor design methods for extreme-scale turbines could result in heavy rotors that negatively impact turbine costs and thus necessitate a different approach to optimize the mass, size, and cost of turbine components. Therefore, robust design methods and an understanding of the dynamics of such extreme-scale wind turbines are necessary.

Various methods exist to design wind turbine rotors. Scaling has been used in the design of research turbines by applying scaling factors to upscale existing smaller turbine designs. At the 25 MW scale, the SUMR-25 two-bladed downwind offshore coned rotor project used technological scaling to scale up the 13.2 MW SUMR-13 rotor in the first of three rotor versions created within that study [8]. Scaling also was used to design a 100 m blade by Sandia National Laboratories using a structural approach to scale up blade geometry and structural properties [9]. Rotors can also be designed without scaling by creating blade geometries (chord and twist distributions) that achieve a desired aerodynamic performance. A direct design approach, sometimes called a design-by-analysis approach, generates a blade geometry first which is then analyzed for performance and subsequently adjusted in an iterative process until a blade geometry that achieves the desired performance emerges. This approach, although often used in the past, is computationally involved and inefficient compared to the inverse design approach that is more commonly used now. With an inverse design approach, parameters for aerodynamic performance such as airfoil characteristics, tip-speed ratio (λ), axial induction factor (a), aerodynamic power (P), and rotor geometry are used as inputs instead of the blade geometry. The blade geometry can then be determined to achieve these desired parameters, eliminating the need to analyze a blade geometry in each iteration as done in the direct design approach, thus saving time and computation resources. This process makes an inverse design approach better suited for designing around a desired peak power production. The inverse approach has been used in the design of both

research and commercial wind turbines and is used in this study. This was accomplished using the multipoint inverse design tool PROPID [10–12]. PROPID has been used for extreme scale rotor design in the SUMR-13i offshore rotor by Ananda et al. and in the aerodynamic redesign of the SUMR-25 rotor as part of the study by Qin et al. [8,13].

Provided that the resulting rotor performs as desired, structural optimization can be performed to minimize mass and cost, and to meet load requirements. The National Renewable Energy Laboratory (NREL) has developed the Wind-Plant Integrated System Design & Engineering Model (WISDEM) framework that is capable of modeling entire turbines and turbine farms [14]. The WISDEM framework is applied in this study to optimize the blade structure given the blade geometry designed in PROPID. Higher fidelity simulations are also useful at this stage to predict the dynamic response and performance of the rotor. The OpenFAST wind turbine simulation framework developed by NREL is a tool that can simulate turbine dynamics using various computational modules for aerodynamics, hydrodynamics, controls, and structural dynamics [15]. Such higher fidelity aeroelastic simulations can provide insight into the loading and deflections a rotor may undergo which can inform rotor geometry design decisions like pre-cone and shaft tilt angles to maximize swept area and thus power production. Qin et al. performed OpenFAST simulations on the redesigned SUMR-25 rotor following a PROPID design phase [8]. Similarly, in this study OpenFAST simulations of the resulting PROPID designs were run with a focus on aeroelastic deflections.

Airfoil selection for wind turbines is another important part of the design process to maximize rotor performance. Ananda et al. used PROFOIL to create the F1 family of airfoils ranging from 18%–48% thickness [13]. These airfoils were based on a design for a 13.2 MW turbine which provide the geometry as a function of the non-dimensional rotor radius (r/R). Characteristics of the F1 airfoils are shown in Fig. 1 and Table 1 at the airfoil design Reynolds number (Re) for the present 25 MW turbine, based on chord length and the relative upstream velocity (based on the combined freestream and rotational components) where the design Re is based on rated conditions (to be described further in Section 2). As these airfoils move outboard (increasing r/R), they have increased aerodynamic efficiency as demonstrated by higher maximum lift-to-drag ratios $(L/D)_{max}$, as listed in Table 1. However, as these airfoils move inboard (decreasing r/R), they have increased thickness-to-chord ratios (t_{max}/c) , which results in increased maximum lift coefficients $(C_{l,max})$ at high angles of attack as shown in Fig. 1. In addition, the inboard airfoils also have increased camber which results in higher lift coefficients at zero angle of attack (C_{l0}) as shown in Fig. 1 and Table 1. Notably, the airfoil shapes for $r/R <$

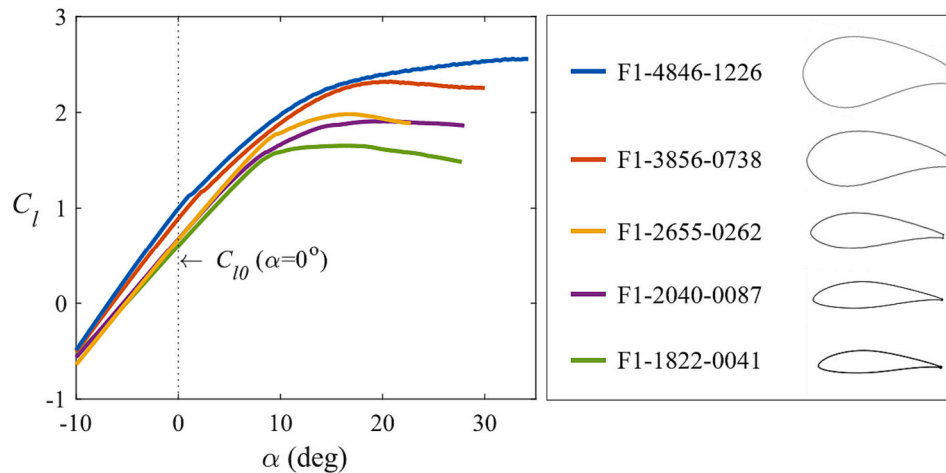


Fig. 1. XFOIL lift curve predictions for the F1 family of airfoils at Reynolds numbers listed in Table 1 at design conditions of the present 25 MW rotor further described in Section 2.

Table 1

F1 airfoil geometries and XFOIL performance characteristics at design Reynolds numbers for the 25 MW rotor.

Airfoil	r/R	Re	$(L/D)_{max}$	t_{max}/c	t_{TE}/c	t_{TE}/t_{max}	C_{l0}
F1-4846-1226	0.25	11.0×10^6	67.5	48.46%	12.26%	0.253	0.997
F1-3856-0738	0.35	11.8×10^6	91.1	38.56%	7.38%	0.191	0.781
F1-2655-0262	0.55	13.0×10^6	172.3	26.55%	2.62%	0.099	0.673
F1-2040-0087	0.75	14.3×10^6	199.7	20.40%	0.87%	0.044	0.640
F1-1822-0041	0.95	12.3×10^6	198.2	18.22%	0.41%	0.023	0.605

0.55 are flatback airfoils. This F1 family of airfoils is also applied in this study for a 25 MW turbine (resulting in larger Reynolds numbers) but with a more formalized optimization based on both aerodynamics and structures, including considering aeroelastic deflections for rotor tilt and coning.

Flatback airfoils have been shown to provide both structural and aerodynamic benefits for larger wind turbine blades near the blade root [16]. The larger cross sections allow for more structural support, and thicker trailing edges reduce premature boundary layer separation, giving flatback airfoils an increased maximum lift coefficient ($C_{l,max}$). For the purpose of designing rotors, the airfoil characteristics of flatback airfoils are used in tools like PROPID in order to achieve the prescribed aerodynamic design parameters like lift coefficient (C_l) distribution and α . These airfoil characteristics can be obtained through numerical tools. The airfoil analysis code XFOIL is used for this purpose in this study [17,18]. However, numerically derived 2-D airfoil characteristics of flatback airfoils have been shown to lack accuracy. XFOIL has been found to mispredict lift and drag coefficients, particularly with the flatback airfoils that are used near the blade root [13,19]. Similarly, 2-D Reynolds-averaged Navier-Stokes (RANS) and unsteady RANS simulations of flatback airfoils have been shown to overpredict $C_{l,max}$ and both over- and underpredict drag coefficients (C_d) which may be attributed to inaccurate modeling of unsteady flow in the wake of the thick trailing edge in 2-D simulations using conventional turbulence models [20–22]. For a robust aerodynamic design, numerically derived airfoil characteristics should be validated using comparable high Reynolds number experimental data to ensure design parameters are realistic. Without such considerations, rotor designs in real operation could lead to shortfalls in performance. Thus, considering adjustments to numerical

airfoil characteristic data is important for the aerodynamic design of physically realizable rotors.

This paper discusses the aerodynamic design of a 25 MW offshore downwind wind turbine rotor with 165 m long blades. The objective of maximizing power production was achieved by maximizing swept area and power coefficient (C_p) while providing experimental validation of design choices. This validation was performed by developing a new empirical correlation to correct numerical airfoil data from XFOIL using experimental flatback airfoil data. The corrected XFOIL data was used to create a design space for prescribing realistic C_l distributions for extreme-scale rotors. Three C_l distributions were then chosen and used to design three different rotors using PROPID, each with different resulting chord (c) and twist (θ) distributions. The performance of each rotor was then assessed using OpenFAST [15] and the WISDEM framework [14] to select the best design. Aeroelastic effects on these extreme scale rotors were also explored.

This paper is the first to present a power-maximizing aerodynamic design for a highly flexible 25 MW rotor that uses experimental flatback airfoil characteristics to consider the high Reynolds number effects that have big implications for rotor design at such extreme scales. This study also considers blade flexibility and tip deflections to prescribe rotor pre-cone and shaft tilt angles to further maximize power production, a strategy not considered in most aerodynamic designs. This study is also one of the first to then analyze the resulting rotor designs using high-fidelity simulations and structural optimization tools to provide more useful predictions of rotor performance and cost for rotors that were aerodynamically designed. Such considerations of scale and blade flexibility are not often seen in aerodynamic designs but are critical for extreme-scale turbine operation. The combination of tools and analyses used in this study provides a better understanding of the design parameters and dynamics of extreme-scale wind turbines and a novel framework for designing these turbines that is a crucial step in the development of offshore wind technology. The following sections will discuss the design methods and considerations as well as the designed rotor performance using numerical simulations.

2. Design methodology

The blade design process began with determining the main design parameters: rotor size, design λ , a , and airfoils. Once the parameters were chosen, PROPID was used to design the rotor geometries. A total of three different blades were designed. These rotor geometries were then analyzed in OpenFAST to study the predictions under steady wind conditions. In the last step, WISDEM was used to minimize blade mass while meeting critical design load cases for each design. This section will

discuss the computational tools and the design parameters selected to design the rotors in this study.

2.1. Computational tools

The PROPID program is a tool for designing and analyzing horizontal axis wind turbines (HAWTs) [10]–[12]. It incorporates a multipoint inverse method that allows the user to specify various desired performance characteristics as input and converge on a blade geometry that achieves the specifications using an iterative solver. Performance characteristics and constraints include peak power, a distribution, C_l distribution, and rated wind speed. PROPID uses blade-element momentum theory through implementing a modified version of the PROP blade-element momentum code, PROPSH. This inverse method can allow one to achieve a desired rotor design much more productively than via a direct design approach. Note that PROPID only considers rigid blades and therefore doesn't account for blade deflection in its design and analysis of HAWTs.

Airfoil characteristics are used as an input in the blade design process within PROPID. Given the airfoils used along the blade span, XFOIL was used to predict 2-D lift and drag coefficients [17,18]. XFOIL data was subsequently processed through the AirfoilPrep preprocessor to create blends of the F1 airfoils and apply 3-D rotational corrections to XFOIL data for PROPID and OpenFAST. AirfoilPrep uses the Du-Selig method for correcting lift and Egger's method for correcting drag [23].

Rotor performance was simulated following the PROPID design stage using OpenFAST, an open-source wind turbine simulation tool developed by NREL [15]. The OpenFAST framework consists of several computational modules coupled to simulate the aerodynamics, hydrodynamics, structural dynamics and controls systems of turbines. Since OpenFAST can simulate time-varying effects and various degrees of freedom, it can provide high-fidelity predictions of these turbine dynamics. OpenFAST can also simulate turbines under unsteady wind conditions, making it useful for simulating design load cases (DLC). However, for the simulations performed in this study, steady wind conditions were used. The aerodynamics module used in OpenFAST was Aerodyn14 which uses blade-element momentum theory for predicting turbine aerodynamics [24].

WISDEM is an open-source integrated system-level design tool, developed by NREL, capable of designing and assessing individual turbines as well as entire wind farms [14]. WISDEM's aerodynamic module is based on blade-element momentum theory. As steady-state models are used in WISDEM, higher fidelity OpenFAST simulations are required for more accurate, time-varying predictions of turbine dynamics. For this study, after separately designing the blade outer mold line using PROPID, WISDEM was used to design and optimize only the internal structures to minimize rotor mass and thus LCOE.

2.2. Main design parameters

The goal of this study was to design a downwind extreme scale wind turbine rotor with a rated power of 25 MW. Design parameters in this study were based partially on the V2e 25 MW turbine described in Escalera Mendoza et al. [25]. The V2e design process involved several steps, going through aerodynamics, structures, and controls analyses. The parameters used in this study are listed in Table 2.

A design tip-speed ratio (λ) of 9.25 was chosen based on tip speed limitations of 120 m/s for offshore turbines. For offshore wind turbines where noise considerations are much less restrictive, an aggressive tip speed limit such as 120 m/s may be appropriate and are already being considered as turbine designs reach these extreme scales [25,26]. The design a was set at the Betz limit of 1/3 along the entire blade span to maximize aerodynamic performance. Blade length and hub radius were based on the rotor sizes previously used in Escalera Mendoza et al. [25]. Blade root thickness was assumed to be 4% of the blade length.

Calculating pre-cone angle and shaft tilt angle required

Table 2

Main design parameters for the 25 MW rotors.

Parameter	Value
Rated power	25 MW
Number of blades	3
Tip-speed ratio	9.25
Target induction factor	1/3
Blade length	165 m
Hub radius	6.75 m
Blade root diameter	6.6 m
Pre-cone angle	6.0°
Shaft tilt	6.0°
Airfoil family	F1

consideration of blade tip deflection (y_{tip}) limits. Using the V2e turbine, the y_{tip} margins toward the tower of a downward pointing blade ($\Psi = 180^\circ$) under the International Electrotechnical Commission (IEC) 61,400–1 standard DLC 1.3 (extreme turbulence model) were considered [27]. The IEC standards define the y_{tip} limit toward the tower as $0.7 \times$ undeflected tip-to-tower distance away from the tower. Using the V2e deflections and the y_{tip} limit definition, the minimum angle that an undeflected blade at $\Psi = 180^\circ$ could be positioned was 12° from vertical. This angle corresponds to the sum of the pre-cone and shaft tilt angles. Next, to determine the individual pre-cone angle and shaft tilt angles, a swept area maximizing approach was used. The approach was to align an upward-pointing blade ($\Psi = 0^\circ$) vertically during operation. Thus, to achieve an upward vertical blade orientation, a pre-cone angle and shaft tilt angle were each set to 6° . Note that these were the pre-cone and shaft tilt angles used in PROPID, which does not consider blade deflections that would deform the blades downwind and decrease swept area during actual operation. A visualization of the rotor geometry can be seen in Fig. 2. Further adjustments to this are described below in the discussion of OpenFAST simulations where these aeroelastic deflections are modeled. It should be noted that this same optimization of tilt and coning angle based on aeroelastic deflections can also be applied to upwind extreme-scale rotors (which are expected to be similarly flexible).

2.3. Flatback airfoil aerodynamic coefficient models

PROPID was used to prescribe not only the a distribution but also the blade C_l distribution along the span. The prescribed C_l distributions are based on the F1 family of airfoils and the Reynolds numbers at which they are operating for the final blade design. Although experimental data for airfoil characteristics would be useful, obtaining such data at the operational Reynolds numbers for extremely large-scale wind

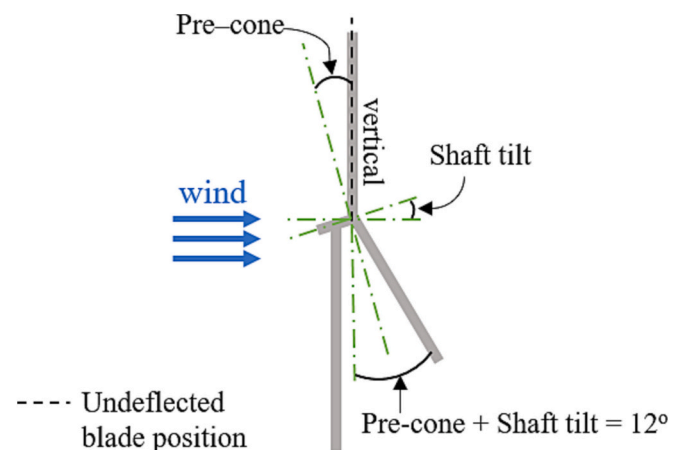


Fig. 2. Pre-cone angle + shaft tilt configurations for PROPID design assuming rigid blades.

turbines would be difficult. Thus, XFOIL was used to predict F1 airfoil performance at Reynolds numbers shown in Table 1. Interpolated aerodynamic coefficients were obtained by interpolating the XFOIL data with Airfoilprep to be used along the blade span in between the r/R locations of the F1 airfoils [23]. The Reynolds numbers used were based on the rated operating conditions of the V2e blade [25].

However, XFOIL has been shown to underpredict C_d for flatback airfoils and overpredict $C_{l,max}$ [13,19]. Due to these discrepancies, XFOIL data is not accurate enough to find the stall point for predicting $C_{l,max}$ and C_d characteristics for flatback airfoils used near the blade root. In order to verify the discrepancies found in previous literature, experimental wind tunnel C_d and C_l data were compared to XFOIL data for the DU97-W-300 airfoil [28–30].

From Fig. 3, it was observed that XFOIL significantly underestimated C_d by $\sim 60\%$ at low angles of attack. Therefore, experimental wind tunnel data was used to empirically adjust XFOIL data to ascertain more accurate C_l and C_d characteristics. The experimental wind tunnel data for various flatback airfoils are shown in Table 3 [29–33]. These data were taken over various Reynolds numbers ranging from 0.76×10^6 to 4×10^6 and had varying trailing edge thicknesses (t_{TE}/c) ranging from 4.2% to 17.5%. These data can be used in conjunction with XFOIL to account for these over/underpredictions.

Experimental flatback airfoil data listed in Table 3 was used to see if any correlation could be found to estimate flatback airfoil C_d before stall. The experimental data showed nearly constant C_d for flatback airfoils in this region. Using this assumption, C_d was found to correlate with the trailing edge ratio (t_{TE}/t_{max}), defined as the ratio of airfoil trailing edge thickness (t_{TE}/c) to airfoil maximum thickness (t_{max}/c), and can be approximately modeled as:

$$C_d = 0.227 \frac{t_{TE}}{t_{max}} - 0.165 \quad (1)$$

This correlation is presented in Fig. 4a. XFOIL data for the F1 family of airfoils is also included in Fig. 4a showing underprediction of C_d compared to the empirical fit. The F1 airfoils with thinner trailing edges did not seem to show as much C_d underprediction and thus XFOIL C_d adjustments were only added to airfoils with $t_{TE}/t_{max} > 0.11$.

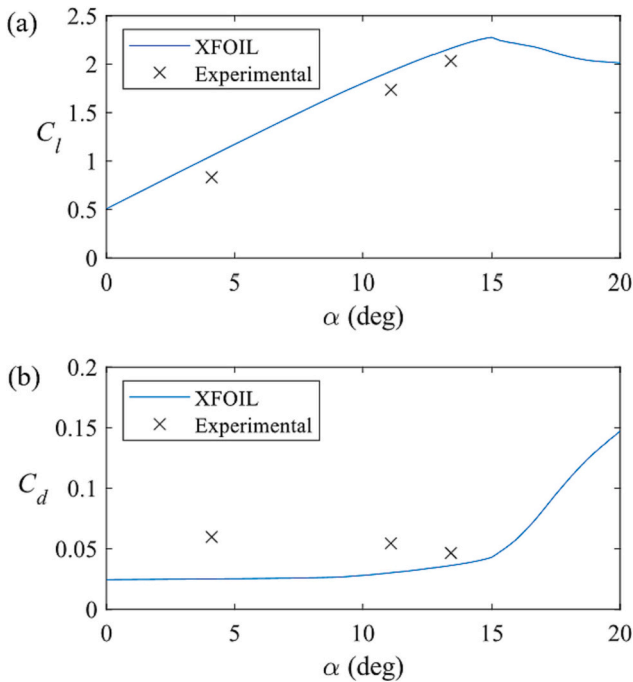


Fig. 3. Comparison of aerodynamic coefficients between XFOIL and experimental data for the DU97-W-300 airfoil at $Re = 3 \times 10^6$ [30] for clean conditions: a) lift; b) drag.

Table 3
Characteristics of experimental flatback airfoils.

Airfoil	t_{max}/c	t_{TE}/c	t_{TE}/t_{max}	$Re (\times 10^6)$	C_{l0}
DU97-W-300 [29,30]	30%	10%	0.333	3	–
LI30-FB10 [31]	30%	10.6%	0.353	1.5	0.16
FB3500–0050 [22]	35%	0.5%	0.014	0.67	0.29
FB3500–0875 [22]	35%	8.75%	0.25	0.67	0.34
FB3500–1750 [22]	35%	17.5%	0.5	0.67	0.51
DU97-W-300 mod. [32]	27%	10%	0.37	1	0.96
FB3500–1750 [21]	35%	17.5%	0.5	0.67	0.36
PGW6 [33]	27%	4.2%	0.155	3	0.46
PGW7 [33]	34%	4.2%	0.123	3	0.48
PGW6 [33]	27%	4.2%	0.155	4	0.48
PGW7 [33]	34%	4.2%	0.123	4	0.47

The experimental data in Table 3 was also used to determine an adjustment for overpredicted XFOIL $C_{l,max}$ data. Since $C_{l,max}$ and C_l at zero angle of attack (C_{l0}) depends on airfoil camber, the C_{l0} of the experimental airfoils was used to determine a correlation for $C_{l,max}$ that can be described as:

$$C_{l,max} = 1.67C_{l0} + 0.52 \quad (2)$$

Again, it was determined for the F1 family of airfoils that the thicker flatback airfoils required adjustment for overpredicted $C_{l,max}$ values, and thus only airfoils with $t_{max}/c > 26.55\%$ (corresponding to the F1–2655–0262 airfoil) were modified.

2.4. Lift coefficient design space and distributions

To set the design C_l distribution used in rotor design, physically realizable values of C_l along the blade span must be determined for the airfoils. This C_l distribution is limited by a margin below the $C_{l,max}$ of the airfoils to consider deviations in angle of attack due to turbulence. To optimize for aerodynamic performance, the C_l distribution should be as close as possible to $(L/D)_{max}$ curve along the blade span. For the F1 family of airfoils, the $C_{l,max}$ and $(L/D)_{max}$ characteristics were calculated using XFOIL data modified by the high Reynolds number $C_{l,max}$ and C_d adjustments described above. These values were then shifted to create the final design space (shown in green in Fig. 5b).

The upper limit of the design space is based on $C_{l,max}$ values and the lower limit is based on C_l values at the $(L/D)_{max}$. These values from XFOIL, without any adjustments, can be seen in Fig. 5a. It can be observed that the flatback airfoils within the inboard 50% of the blade show very high $C_{l,max}$ values as well as low $(L/D)_{max}$ values due to underpredicted C_d before stall. Accounting for C_d and $C_{l,max}$ adjustments, the $C_{l,max}$ vs. $(L/D)_{max}$ curves can be seen in Fig. 5b, showing decreased $C_{l,max}$ values and increased $(L/D)_{max}$ values for the inboard flatback airfoils.

From the $C_{l,max}$ and $(L/D)_{max}$ curves, adjustments could then be made to create the final design space. The upper limit of the design space was created by uniformly decreasing the $C_{l,max}$ curve by 0.2 as shown in Eq. 3 to create a margin for excursions in angle of attack due to turbulence. The lower limit was created by adjusting the $(L/D)_{max}$ curve by a factor of 0.6 as shown in Eq. 4, low enough to encompass the $(L/D)_{max}$ curve, thus creating a reasonable bracket for C_l distributions. The upper and lower C_l limits of the final design space can then be described as:

$$C_{l,upper} = C_{l,max} - 0.2 \quad (3)$$

$$C_{l,lower} = 0.6(L/D)_{max} \quad (4)$$

From this design space, three C_l distributions were determined for three different rotor designs presented in Fig. 6. The three distributions were placed at the upper, middle, and lower parts within the design space. The Design 3 distribution is the same distribution used in the V2e rotor design and was kept the same as a method of comparison to the two other cases [25]. All the distributions decrease linearly from $r/R = 0.25$

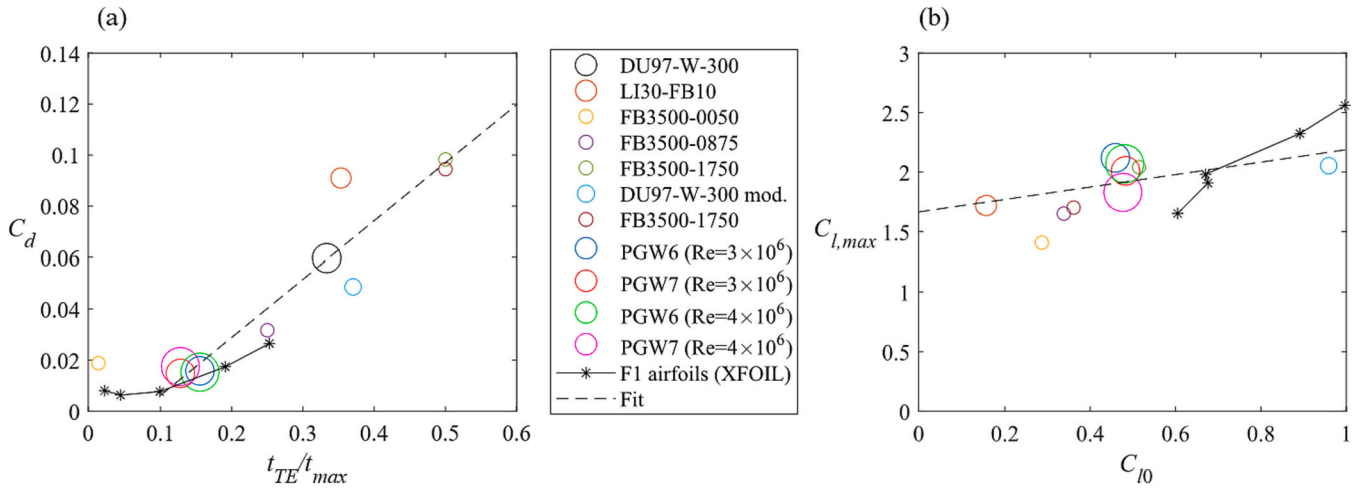


Fig. 4. Flatback (a) drag and (b) maximum lift coefficient correlations. Larger marker size corresponds to larger Reynolds number. Order of listed airfoils is the same as in Table 3.

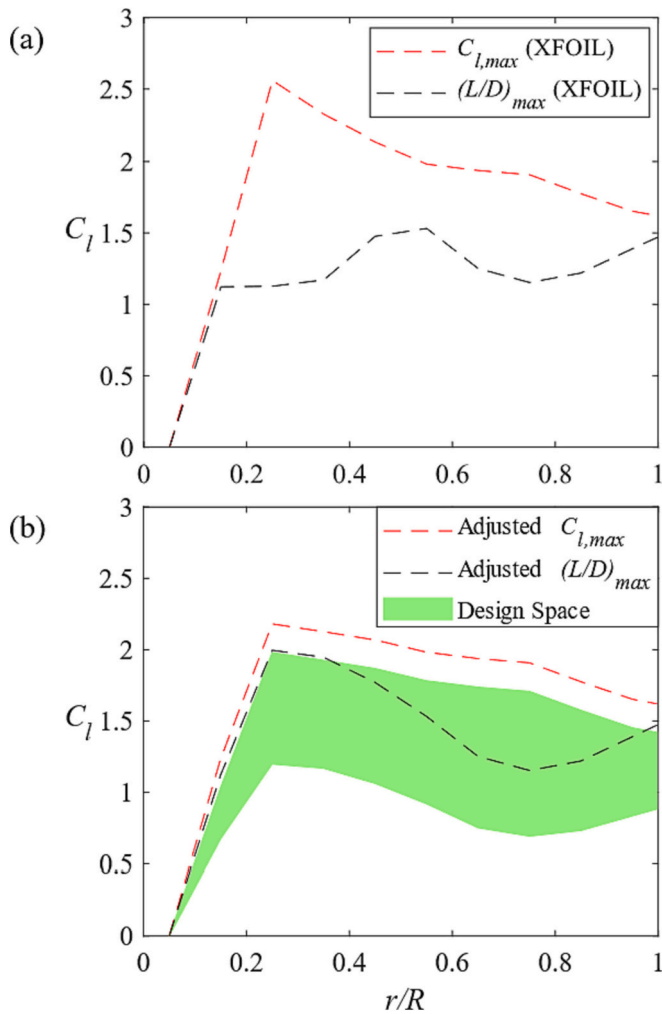


Fig. 5. a) XFOIL maximum lift coefficient and lift-to-drag ratio curves of F1 airfoils for clean conditions; b) final design space and empirical lift coefficient limits with adjustments.

to the blade tip. While the ideal aerodynamic performance would be achieved on the $(L/D)_{max}$ curve, the linear C_l distributions chosen allow for smoother chord distributions, and in case of Designs 1 and 2, the C_l

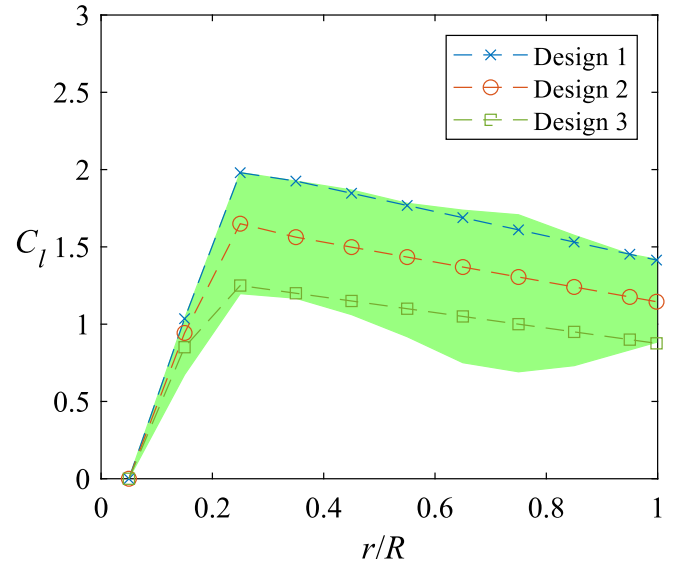


Fig. 6. Lift coefficient distributions of Designs 1–3 within the final design space for clean conditions (free transition).

distributions contain sections that overlap the $(L/D)_{max}$ curve. A similar strategy was used in the design of a 15 MW rotor with a similar rotor diameter that also achieved a chord distribution very close to optimum L/D [34]. These differences between the C_l distributions of Designs 1–3 lead directly to differences in blade chord and twist that could then be run in simulations to compare performance.

It should be noted that this design space has been created assuming clean blade surface conditions. This was done by using the e^N transition method with $N = 9$ in XFOIL when producing the F1 airfoil data [17]. However, turbine blades in actual operation will experience surface degradation overtime that can significantly increase roughness and cause premature boundary layer transition which is a cause for concern for aerodynamic performance. To maintain the usefulness of the design space shown in Fig. 5b, XFOIL data was also obtained for an early transition case ($N = 0.3$) and a fully turbulent case (forced transition at the leading edge) and then used to create two more design spaces using the same methodology and empirical adjustments described above. Polars of the F1 airfoil characteristics and transition location of three sets of XFOIL data are shown in Fig. 7 and Fig. 8 respectively.

The two premature transition cases showed decreased C_l and

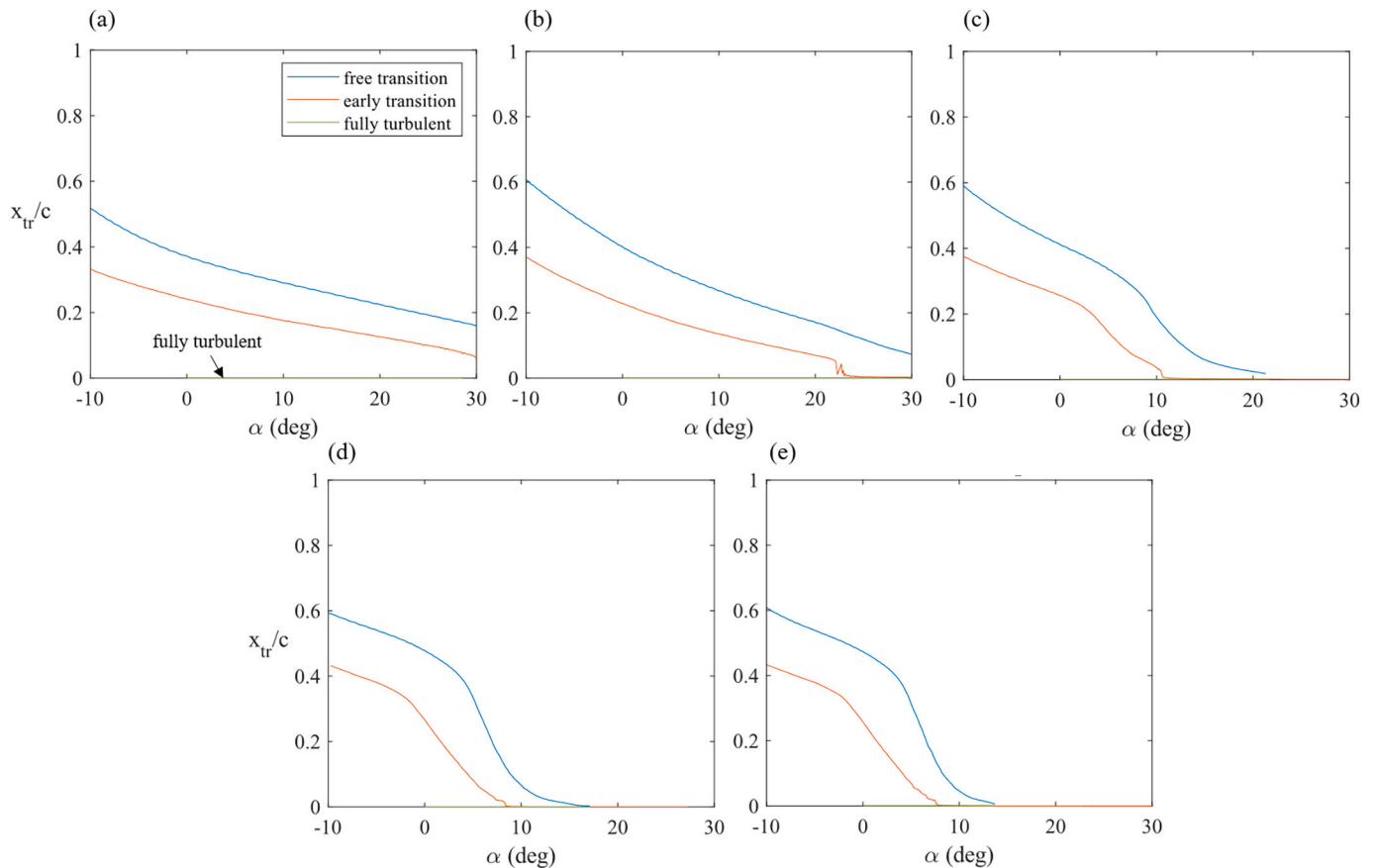


Fig. 7. Airfoil transition location normalized by chord for F1 airfoils for varying angles of attack and three transition criteria. a) F1-4846-1226; b) F1-3856-0738; c) F1-2655-0262; d) F1-2040-0087; e) F1-1822-0041. Note that $x_{tr}/c = 0$ for fully turbulent conditions on each airfoil.

increased C_d as expected with the thicker flatback airfoils showing the most loss in aerodynamic performance. The $C_{l,max}$ and $(L/D)_{max}$ curves using just the XFOIL data are shown in Fig. 9a for all three transition cases. However, using the adjustments in Eq. 1–4 to create a C_l design space adjusts the thicker flatback airfoil characteristics where the most aerodynamic performance loss occurs. The resulting 3 design spaces shown in Fig. 9b span similar ranges of C_l that do not differ as significantly as the $C_{l,max}$ and $(L/D)_{max}$ curves shown in Fig. 9a, although the design spaces of the early transition and fully turbulent cases appear to be shifted slightly toward lower C_l values compared to that of the free transition case used in this study. Future designs may further consider these surface degradation effects in prescribing C_l distributions.

3. Results and discussion

3.1. PROPID results

The parameters listed in Table 2 were inputs in PROPID for three separate cases, each with one of the three C_l distributions shown in Fig. 6. The PROPID results are shown in Fig. 10. The axial induction factor of $1/3$ across the blade span in Fig. 10a indicates that the prescribed a was successfully converged upon in each of the three designs.

The chord distributions for Designs 1–3 in Fig. 10b show Design 1 with the smallest chord distribution and Design 3 with the largest chord distribution, as expected given that chord is inversely related to C_l . All three designs show maximum chord values between $r/R = 0.15$ – 0.25 with Design 3 having a maximum chord approximately 60% larger than that of Design 1.

Twist distributions shown in Fig. 10c are similar between Designs 1–3 (note that greater positive twist angle twists the blade into feather).

Between $r/R = 0.15$ – 1.0 , Designs 2 and 3 smoothly decrease from $\sim 24^\circ$ to slightly negative angles past $r/R = 0.75$. However, in Design 1, twist starts to increase past $r/R = 0.75$. This twist increase occurs because the prescribed C_l values at those locations required less angle of attack than would occur if the twist distribution were to continue decreasing smoothly as is the case in Designs 2 and 3. Because the trends in twist at the blade tip appear in order from Design 1 to Design 3, and since the Design 1 C_l distribution is already at the upper limit of the design space, Design 1 was left unchanged. A 1:1 scale rendering of the three designs is shown in Fig. 11 as a more realistic view of the blade geometries.

The PROPID results for blade pitch angle (β), maximum power coefficient ($C_{p,max}$), and thrust coefficient (C_T) are shown in Table 4. The blade pitch angle refers to the pitch in angle in Region 2 of the power curve to get the desired aerodynamic performance and is in reference to $r/R = 0.75$ where blade twist is zero. The $C_{p,max}$ and C_T values are calculated at the design λ of 9.25.

3.2. OpenFAST simulations

The three designs were subsequently analyzed in OpenFAST to compare performance predictions and observe aeroelastic effects on power and thrust. The process of running OpenFAST, and its results will be discussed in the following subsections.

3.2.1. OpenFAST parameters

All simulations were performed using steady wind speeds in Region 2 (5 m/s to U_{rated}) neglecting shear and without a controller. Simulations were performed at each wind speed for a sufficiently long time in order to ignore initial transient effects in OpenFAST. Rotor speed was held constant at each wind speed such that the design λ of 9.25 was

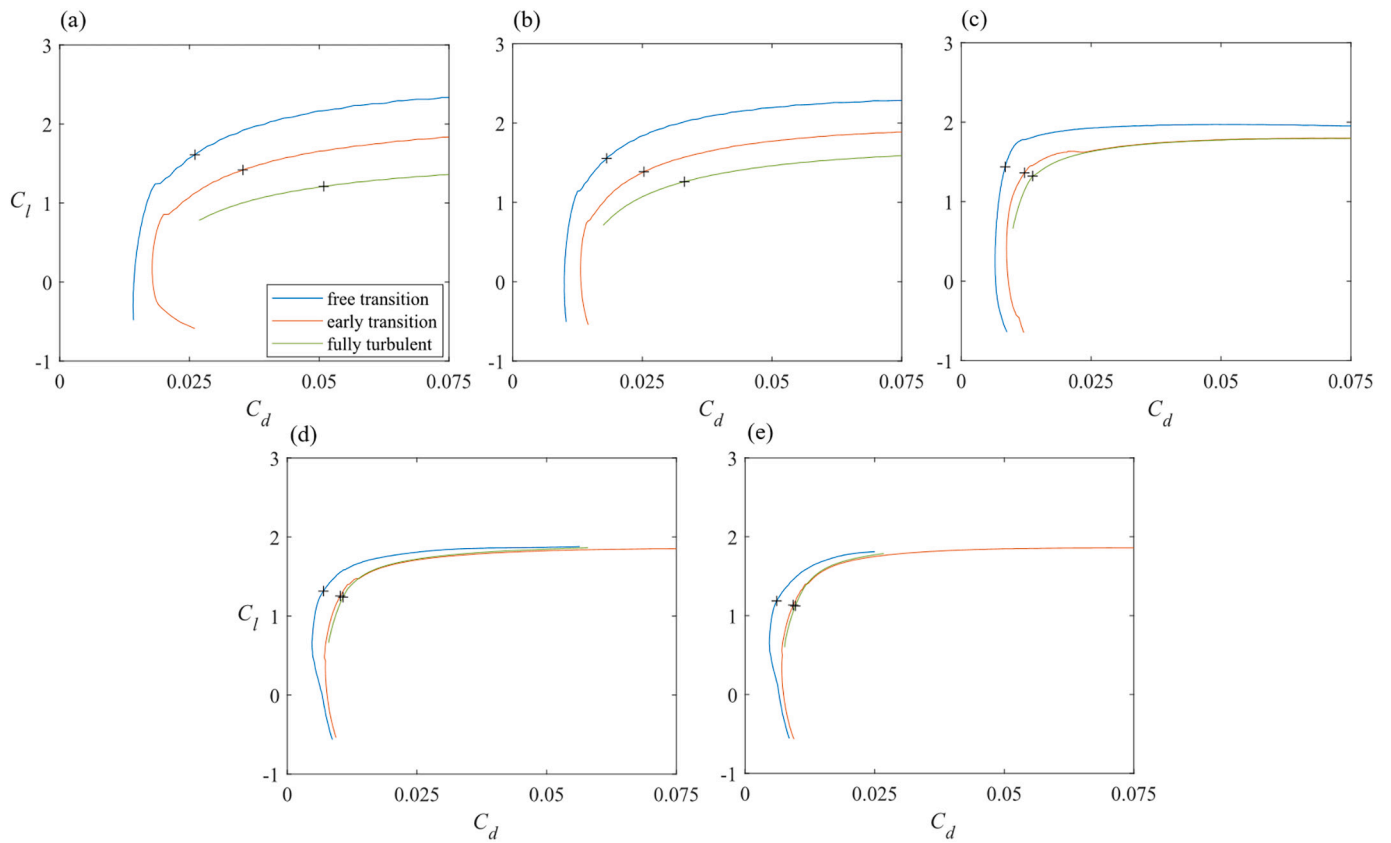


Fig. 8. Polars of the F1 family airfoils for three different transition criteria produced using XFOIL, where ‘+’ marks operating points at rated conditions of Design 2 for each transition criteria. a) F1-4846-1226; b) F1-3856-0738; c) F1-2655-0262; d) F1-2040-0087; e) F1-1822-0041.

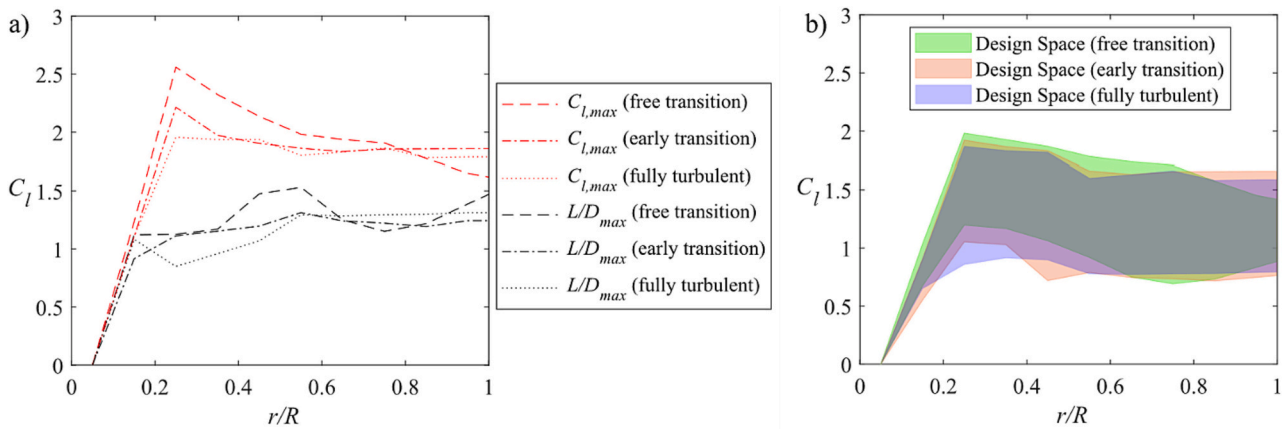


Fig. 9. a) XFOIL maximum lift coefficient and lift-to-drag ratio curves of F1 airfoils for three different transition criteria; b) Empirical lift coefficient limits with adjustments and resulting design spaces for the three different transition criteria.

maintained, and β values from PROPID (shown in Table 4) were used. For aerodynamic loads, the Aerodyn 14 module was used [24]. The V2e tower design and blade structural properties from Escalera Mendoza et al. [25] were used for all three rotors. Finally, both rigid and flexible blade cases were considered.

3.2.2. Flexible blade adjustment

As described previously, a design strategy was to maximize swept area by minimizing pre-cone and tilt angle while maintaining tip-deflection margins defined by the IEC 61400-1 standards as well as aligning the blades at $\Psi = 0^\circ$ to be vertical. To achieve this in operation,

blade deflections must be considered as they will change the blade alignment and thus swept area. Therefore, for OpenFAST simulations with flexible blades, the pre-cone and shaft tilt angles were changed to allow aeroelastic orientation of the blade at $\Psi = 0^\circ$ to be nearly vertical when deflected downwind resulting in a blade pointing slightly upwind at $\Psi = 0^\circ$ when rigid as can be seen in Fig. 12. This adjustment was based on the average blade deflections observed in flexible blade simulations at $\Psi = 0^\circ$ and at a high Region 2 wind speed ($U = 8$ m/s) with the V2e turbine. The rigid blade configuration is the same one shown in Fig. 2 above. The 8 m/s velocity was used based on the assumption that the turbine will be operating in this upper range of Region 2 for a majority of

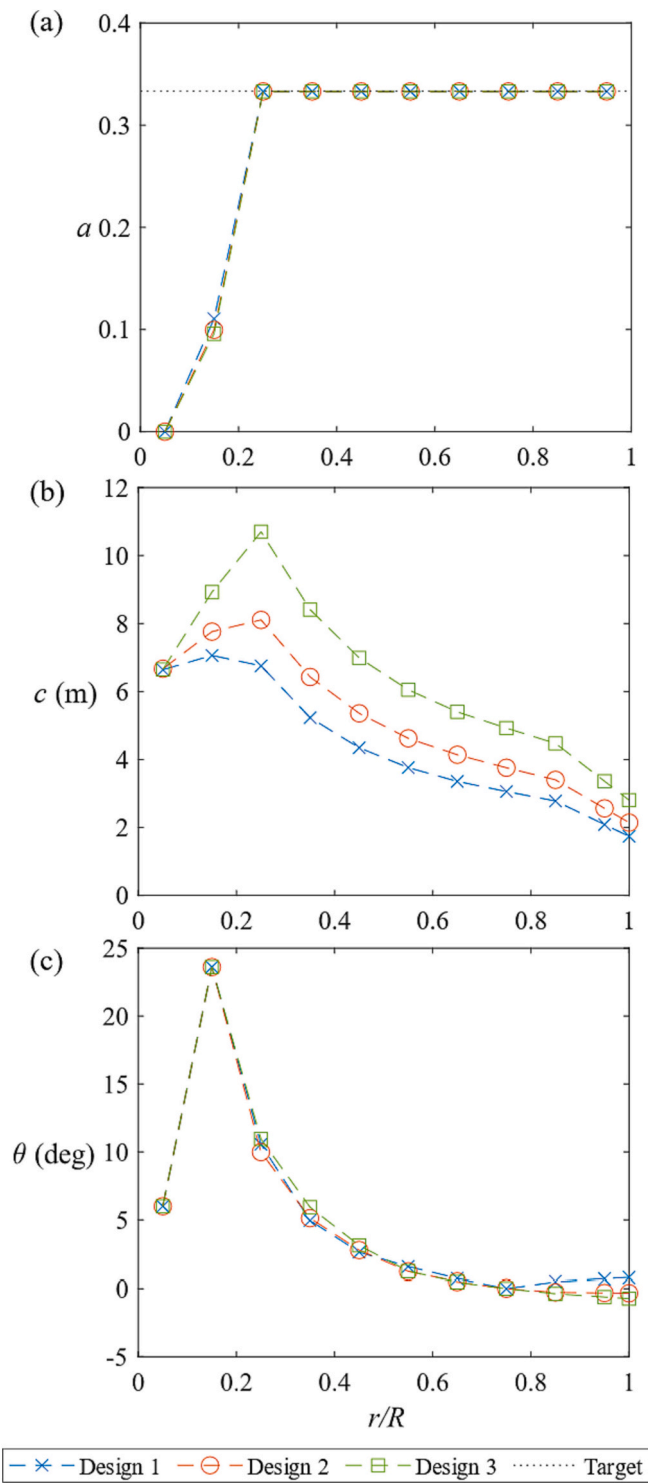


Fig. 10. PROPID results for Designs 1–3 along nondimensional blade span: a) axial induction factor; b) chord; c) twist.

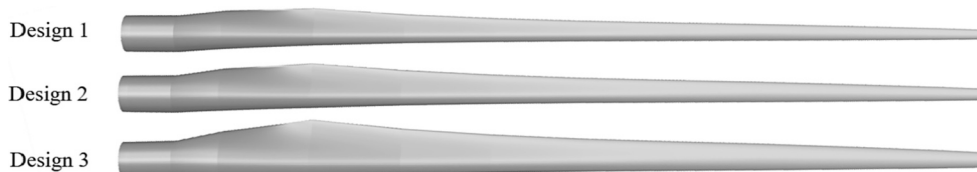


Fig. 11. 3-D rendered blades for Designs 1–3.

its time. Thus, adjusting for the deflections at 8 m/s would allow for the swept area to be near maximum as much as possible. However, the combination of pre-cone angle and shaft tilt angle was kept at 12° to prevent tower strike.

When the performance of the flexible blade configuration is compared to that of the rigid blade configuration, initially less power will be produced at lower Region 2 wind speeds as the rotor swept area will be smaller due to the upward pointing blade still being slightly upwind. But at higher Region 2 wind speeds, the flexible blade configuration will be able to produce more power as the near vertical blade will create a larger swept area than the rigid blade configuration that has a deflected upward pointing blade pointing downwind.

Table 5 shows these adjusted pre-cone and shaft tilt angles for the aeroelastic designs. There is only a 0.2% decrease in C_P and a 2.5% decrease in C_T due to aeroelastic deflections at a steady, no-shear 8 m/s wind. However, these differences may differ with turbulence and shear included.

3.2.3. OpenFAST results

For rigid blade simulations, the OpenFAST results for a and C_l

Table 4

Blade pitch angle and rotor performance (PROPID).

	Pitch angle (β)	$C_{P,max}$ (PROPID)	$C_T @ C_{P,max}$ (PROPID)
Design 1	-3.91°	0.505	0.825
Design 2	-0.02°	0.511	0.823
Design 3	2.79°	0.510	0.823

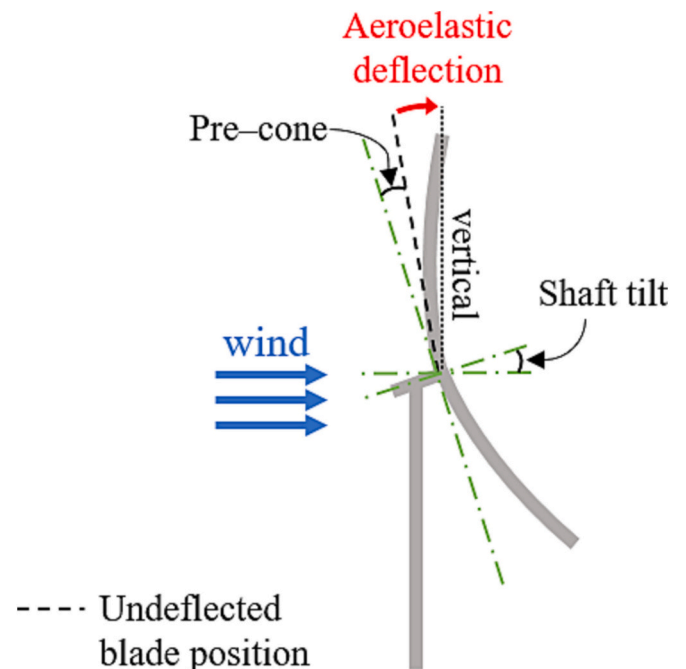


Fig. 12. Pre-cone angle + shaft tilt configurations for flexible blade OpenFAST simulations.

Table 5
Rigid and flexible blade configurations.

	Rigid design	Aeroelastic design
Pre-cone angle	6°	3.6°
Operation cone angle	6°	7.8°
Shaft tilt angle	6°	8.4°
Pre-cone swept area [m ³]	91.81 × 10 ³	91.33 × 10 ³
Operation swept area [m ³]	91.81 × 10 ³	89.80 × 10 ³
C_P	0.498	0.496
C_T	0.836	0.815

(prescribed parameters in PROPID) were verified to match the desired targets within 1%. All three designs produced similar power, but Design 2 provided the most power, producing 0.9% more than Design 1 and 0.7% more than Design 3 on average over the simulated wind speeds. Design 1 shows the highest rated thrust (T_{rated}) at 4.26 MN: 0.2% more than Design 3 and 0.7% more than Design 2. These results of aerodynamic power and thrust are consistent with the PROPID results which showed Design 2 with the highest $C_{P,max}$ of 0.511 and Design 1 with the highest C_T @ $C_{P,max}$ of 0.825. Average thrust across wind speeds decreased in the order of decreasing C_l distribution (i.e., Design 1 had the highest average thrust and Design 3 the lowest).

The aeroelastic effects on power and thrust are shown in Fig. 13. As the blades deflect downwind, the rotor swept area decreases, effectively reducing the power production and thrust forces on the rotor. The

results for Design 2 show a power loss between 1.4%–4.7% across wind speeds with the greatest loss at U_{rated} when compared to the rigid rotor. Likewise, T_{rated} decreases by 1.4% from 4.23 MN to 4.17 MN, but the reduction in thrust ranged from 0.4%–1.4% across wind speeds. Designs 1 and 3 also showed similar performance for power and thrust.

Tip deflections for Design 2 in the flexible blade configuration are shown in Fig. 14. Figure 14a shows downwind tip deflections at $U = 8$ m/s varying from 11 to 14.1 m with maximum deflections occurring when the blade is at $\Psi = 0^\circ$. As mentioned before, adjustments for pre-cone and shaft tilt angles for blade flexibility were based on average tip deflections observed at $U = 8$ m/s in the V2e turbine. However, the deflection observed in V2e was ~2 m larger than that observed in Designs 1–3. This meant that at $U = 8$ m/s the upward pointing blade for Designs 1–3 was slightly less vertical than desired and rather reached a more vertical position closer to $U = 9$ m/s. This difference may be corrected in a future iteration to further improve performance. Solely considering steady Region 2 wind speeds, y_{tip} limits specified by IEC standards were not violated, although more considerable deflections that would push these limits are often seen with extreme gust conditions such as DLC 1.4.

3.3. WISDEM results

In the final part of this study, the three rotor designs were evaluated using WISDEM to optimize for minimal rotor mass and LCOE. Since the WISDEM optimization was performed after the OpenFAST simulations, the resulting WISDEM structural properties are different from the more detailed V2e blade structural design by Escalera Mendoza et al. used in

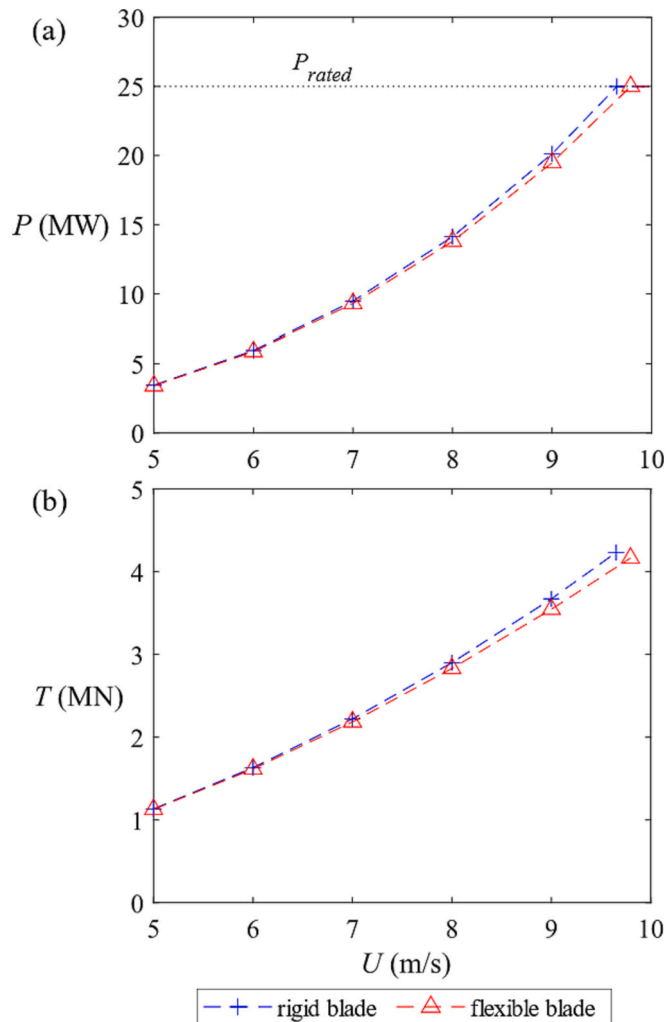


Fig. 13. Aeroelastic effects on Design 2 with steady wind (OpenFAST): a) aerodynamic power; b) aerodynamic thrust.

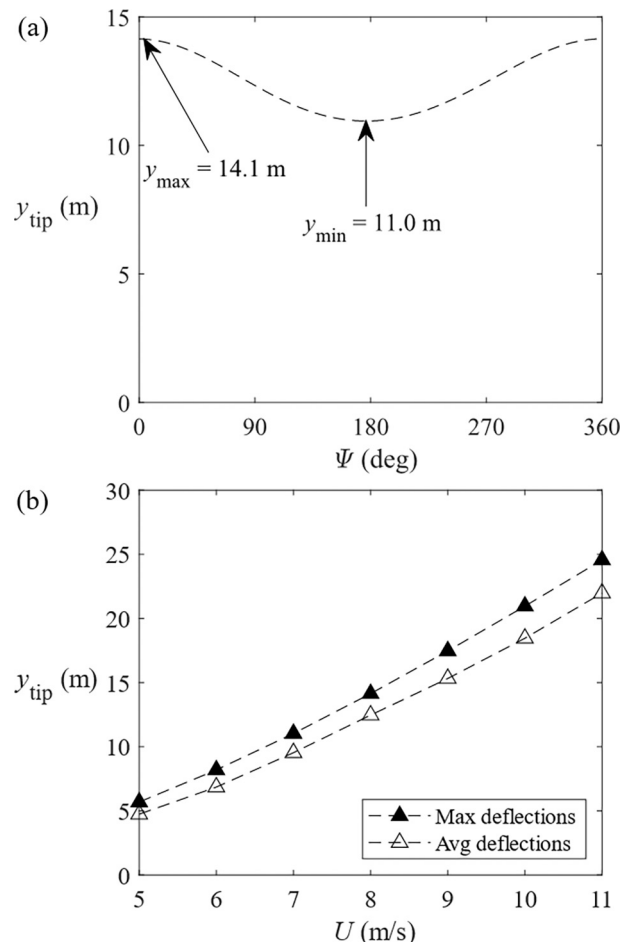


Fig. 14. Downwind tip deflections on Design 2 blade (OpenFAST): a) at 8 m/s steady wind (vertical blade at $\Psi = 0^\circ$); b) 5–11 m/s steady winds.

the OpenFAST simulations [25]. While creating higher fidelity structural designs for all three rotors would be ideal to use in the OpenFAST simulations, for purposes of this study, such structural designs were not performed due to time and resource constraints. However, the use of WISDEM allowed for more rapid estimates of structural design. By constraining the blade geometry, the WISDEM optimization can still provide a useful approximation of a blade structural design to compare the effects of varying chord and twist distributions on blade mass and LCOE. Results can be seen in Table 6. WISDEM was first run using a strain constraining approach, optimizing structures to a typical limit of 4000 micro-strain due to flapwise and edgewise blade loads under extreme wind conditions [26,35]. Spar cap thickness as well as leading edge and trailing edge thicknesses were the drivers of the structural design. This approach was used for the blade structural design in Escalera Mendoza et al. [25]. The strain constrained approach resulted in Design 1 exhibiting the lightest blade mass and lowest LCOE most likely due to the smallest chord in Design 1. However, this approach also resulted in downwind tip deflections >50 m for Designs 1 and 2 that surpassed downwind tip-deflection limits. Thus, the WISDEM approach was updated to constrain deflections in addition to strain. This deflection limit was based on the downwind deflection limits from the IEC standards for an upwind version of the V2e rotor [25,27].

These results showed an increased blade mass for Designs 1 and 2 but much more reasonable tip deflections. LCOE for the deflection constrained rotors also increased for Designs 1 and 2 as stiffer and heavier blades require more material. However, blade mass and LCOE for Design 3 decreased between the strain constrained rotor and the deflection constrained rotor, also resulting in higher tip deflections.

The tip-deflection constrained WISDEM results indicate Design 2 as the lightest and least expensive rotor. This rotor is the same design that showed the highest aerodynamic power in the OpenFAST simulations and the highest $C_{p,max}$ from PROPID. The results in AEP and mass (hence LCOE) indicate Design 2 as being the best of the three rotors. The high $C_{p,max}$ and moderate chord of Design 2 likely benefited the resulting LCOE by increasing AEP and limiting blade mass and thus costs to a moderate degree. Based on these results, of the three rotors designed in this study, Design 2 can be recommended for use in further studies of 25 MW offshore turbines including further structures analyses and controls design.

4. Conclusions

The benefits of continuously increasing offshore wind turbine scales call for extreme scale rotor designs that can maximally produce power. In this study, the aerodynamics of three different blade geometries were strategically designed using PROPID and compared through numerical simulations in OpenFAST and WISDEM for a 25 MW downwind rotor. This included a new optimization approach for the flexible blade configuration to consider optimum rotor tilt and coning based on aeroelastic deflections at sub-rated conditions as well as a blade aerodynamic geometry that employs a design space based on a combination of maximum lift and maximum L/D with the design objective to both maximize power production and minimize rotor mass, so as to minimize the LCOE. Creating this design space required determining new empirical correlations based on experimental wind tunnel data to adjust inaccurate 2-D XFOIL data of the flatback airfoils used near the blade root. Three different rotor designs, each with different C_l distributions, were evaluated, first adjusting the rotor designs to maximize swept area without violating tip-deflection constraints and thus maximizing power. OpenFAST was then used to predict desired performance and compare Designs 1–3. Finally, WISDEM was used to optimize for minimal rotor mass, and hence LCOE, while maintaining constraints on maximum tip-deflection and blade strain. The blade strain constrained cases and the maximum tip-deflection constrained cases showed different results in blade mass, a finding that could be important to consider in future studies. The three different design stages (PROPID, OpenFAST,

Table 6
WISDEM blade mass optimization results.

	Design	AEP (GWh/yr)	LCOE (\$/MWh)	m_{blade} (kg)	Y_{tip} (m)
Strain Constrained	1	135.2	71.88	1.281×10^5	59.95
	2	135.8	72.36	1.380×10^5	50.16
	3	135.5	73.53	1.586×10^5	40.18
Deflection Constrained	1	135.2	73.89	1.598×10^5	41.74
	2	135.8	72.72	1.450×10^5	41.63
	3	135.5	73.25	1.532×10^5	41.75

WISDEM) performed in sequence provided a strategy for determining the best performing design, and all indicated that Design 2 was the preferred rotor due to the following results: highest $C_{p,max}$ from PROPID, highest power production in OpenFAST, lightest blade and lowest LCOE from WISDEM. Thus, the final 25 MW design was completed.

This study represents the first step in the aerodynamic design of highly flexible, downwind, extreme-scale 25 MW rotors, but can be applied to upwind extreme-scale rotors as well. As the focus of this study was on rotor aerodynamics, more work needs to be done on the structural and controls system aspects of these rotor designs. While this design process relied on predicting steady inflow wind performance, the careful consideration of design parameters in this study leads to the expectation that these rotors will still perform well under more realistic and extreme wind conditions. However, further simulations are recommended to assess this. A control system design study will be performed on the final rotor design developed in this paper which considers DLCs and incorporates an active IPC control system to better evaluate the performance of this rotor under more realistic wind conditions. Future studies on a more detailed structural design for this 3-bladed 25 MW rotor are also recommended. Future work may also focus on trade studies of pre-cone and shaft tilt angles to provide more benefit in power.

CRedit authorship contribution statement

Michael Jeong: Writing – review & editing, Writing – original draft, Visualization, Validation, Methodology, Investigation. **Eric Loth:** Writing – review & editing, Writing – original draft, Supervision, Project administration, Methodology, Funding acquisition, Conceptualization. **Chris Qin:** Writing – review & editing, Writing – original draft, Supervision, Methodology, Investigation. **Michael Selig:** Writing – review & editing, Writing – original draft, Supervision, Methodology, Investigation, Funding acquisition, Conceptualization. **Nick Johnson:** Writing – review & editing, Writing – original draft, Investigation.

Declaration of Competing Interest

The authors declare that they have no known competing financial interests or personal relationships that could have appeared to influence the work reported in this paper.

Data availability

Data will be made available on request.

Acknowledgements

We would like to acknowledge GE Research and Advanced Research Projects Agency-Energy (ARPA-E), U.S. Department of Energy, for support and input throughout the course of this project as well as ARPA-E

for the funding in part under Award Number DE-AR0000667. This work was authored in part by the National Renewable Energy Laboratory, operated by Alliance for Sustainable Energy, LLC, for the U.S. Department of Energy (DOE) under Contract No. DE-AC36-08GO28308. Funding provided by U.S. Department of Energy Advanced Research Projects Agency-Energy. The views expressed in the article do not necessarily represent the views of the DOE or the U.S. Government. The U.S. Government retains a nonexclusive, paid-up, irrevocable, worldwide license to publish or reproduce the published form of this work. M. J. would also like to acknowledge support from the National Science Foundation Research Traineeship (NRT) program under Grant No. 1829004.

References

- [1] U.S. Department of Energy (DOE). Wind vision: a new era for wind power in the United States. 2015.
- [2] The White House. Biden Administration Jumpstarts Offshore wind energy projects to create jobs [accessed April, 2023], <https://www.whitehouse.gov/briefing-room/statements-releases/2021/03/29/fact-sheet-biden-administration-jumpstarts-offshore-wind-energy-projects-to-create-jobs/>; 2021.
- [3] Siemens Gamesa Renewable Energy. Powered by change: siemens gamesa launches 14 offshore direct drive turbine with 222-meter rotor. Press Release [accessed February, 2022], <https://www.siemensgamesa.com/en-int/-/media/siemensgamesa/downloads/en/newsroom/2020/05/siemens-gamesa-press-release-turbine-14-222-dd-en.pdf>; 2020.
- [4] Shields M, Beiter P, Nunemaker J, Cooperman A, Duffy P. Impacts of turbine and plant upsizing on the levelized cost of energy for offshore wind. *Appl Energy* 2021; 298:117189. <https://doi.org/10.1016/j.apenergy.2021.117189>.
- [5] Loth E, Steele A, Qin C, Ichter B, Selig MS, Moriarty P. Downwind pre-aligned rotors for extreme-scale wind turbines. *Wind Energy* 2017;20:1129–311. <https://doi.org/10.1002/we.2092>.
- [6] Costoya X, DeCastro M, Carvalho D, Gómez-Gesteira M. On the suitability of offshore wind Energy resource in the United States of America for the 21st century. *Appl Energy* 2020;262:114537. <https://doi.org/10.1016/j.apenergy.2020.114537>.
- [7] Caglayan DG, Ryberg DS, Heinrichs HU, Linssen J, Stolten D, Robinius M. The techno-economic potential of offshore wind energy with optimized future turbine designs in Europe. *Appl Energy* 2019;255:113794. <https://doi.org/10.1016/j.apenergy.2019.113794>.
- [8] Qin C, Loth E, Zalkind D, Pao L, Yao S, Griffith T, et al. Downwind coning concept rotor for a 25 MW offshore wind turbine. *Renew Energy* 2019;156:314–27. <https://doi.org/10.1016/j.renene.2020.04.039>.
- [9] Griffith TD, Ashwill TD. The Sandia 100-meter all-glass baseline wind turbine blade: SNL100-00. Technical Report SAND2011-3779. Sandia National Laboratories; 2011.
- [10] Selig MS, Tangler JL. Development and application of a multipoint inverse design method for horizontal Axis wind turbines. *Wind Eng* 1995;19(5):91–105.
- [11] Selig MS. PROPID for horizontal axis wind turbine design. <https://m-selig.ae.illinois.edu/propid.html>; 1995.
- [12] Selig MS. PROPID user manual version 5.3.1. UIUC Applied Aerodynamics Group; 2012.
- [13] Ananda GK, Bansal S, Selig MS. Aerodynamic design of the 13.2 MW SUMR-13i wind turbine rotor. AIAA Paper 2018-0094. In: Wind energy symposium; 2018. <https://doi.org/10.2514/6.2018-0994>.
- [14] NREL. WISDEM, v3.2.0. GitHub [code] available at: <https://github.com/WISDEM/WISDEM>; 2023.
- [15] NREL. OpenFAST, v2.5.0. GitHub [code], available at: <https://github.com/OpenFAST/openfast>; 2023.
- [16] TPI Composites, Inc. Innovative design approaches for large wind turbine blades. Technical Report SAND2004-0074. Sandia National Laboratories; 2004. <https://doi.org/10.2172/809617>.
- [17] Drela M. XFoil: an analysis and design system for low Reynolds number airfoils. Low Reynolds Numb Aerodyn Lect Notes Eng 1989;54:1–12. https://doi.org/10.1007/978-3-642-84010-4_1.
- [18] Drela M. XFoil subsonic airfoil development system [accessed April, 2021], <http://web.mit.edu/drela/Public/web/xfoil/>; 2000.
- [19] Coder JG, Maughmer MD. Comparisons of theoretical methods for predicting airfoil aerodynamic characteristics. *J Aircr* 2014;51(1):183–91. <https://doi.org/10.2514/1.C032232>.
- [20] Stone C, Barone M. A computational study of the aerodynamics and aeroacoustics of a flatback airfoil using hybrid RANS-LES. AIAA Paper 2009-273. In: 47th AIAA aerospace sciences meeting; 2009. <https://doi.org/10.2514/6.2009-273>.
- [21] Metzinger CN, Chow R, Baker JP, Cooperman AM, van Dam CP. Experimental and computational investigation of blunt trailing-edge airfoils with splitter plates. *AIAA J* 2018;56:3229–39. <https://doi.org/10.2514/1.J056098>.
- [22] Baker JP, Mayda EA, van Dam CP. Experimental analysis of thick blunt trailing-edge wind turbine airfoils. *J Solar Energy Eng* 2006;128:422–31. <https://doi.org/10.1115/1.2346701>.
- [23] Ning SA. AirfoilPrep.py documentation release 0.1.0. NREL/TP-5000-58817. Golden, CO (US): National Renewable Energy Laboratory; 2013.
- [24] Moriarty PJ, Hansen AC. AeroDyn theory manual. NREL/TP-500-36881. Golden, CO (US): National Renewable Energy Laboratory; 2005.
- [25] Escalera Mendoza AS, Griffith DT, Qin C, Loth E, Johnson N. Rapid approach for structural design of the tower and monopile for a series of 25 MW offshore turbines. In: The science of making torque from wind (TORQUE 2022); 2022. <https://doi.org/10.1088/1742-6596/2265/3/032030>.
- [26] Yao S, Cheta M, Griffith TD, Escalera Mendoza AS, Selig MS, Martin D, et al. Aero-structural design and optimization of 50 MW wind turbine with over 250-m blades. *Wind Eng* 2022;46:273–95. <https://doi.org/10.1177/0309524X211027355>.
- [27] International Electrotechnical Commission. IEC 64100-1, third Ed. 2005-2008, wind turbines – Part I: Design requirements. IEC; 2005.
- [28] Timmer WA, van Rooij RPJOM. Summary of the delft university wind turbine dedicated airfoils. *J Solar Energy Eng* 2003;124:488–96. <https://doi.org/10.1115/1.1626129>.
- [29] Berg D, Barone MF. Aerodynamic and acoustic properties of a flatback airfoil (will it rumble or whisper). Technical Report SAND2008-4306P. Sandia National Laboratories; 2008.
- [30] Barone MF, Berg D. Aerodynamic and aeroacoustic properties of a flatback airfoil: an update. Technical Report SAND2008-8243C. Sandia National Laboratories; 2008. <https://doi.org/10.2514/6.2009-271>.
- [31] Manolesos M, Voutsinas SG. Experimental study of drag-reduction devices on a Flatback airfoil. *AIAA J* 2016;54:3382–96. <https://doi.org/10.2514/1.J054901>.
- [32] Yilmaz O, Timmer WA. Experimental evaluation of a non-conventional flat back thick airfoil concept for large offshore wind turbines. AIAA Paper 2018-3827. In: AIAA applied aerodynamic conference; 2018. <https://doi.org/10.2514/6.2018-3827>.
- [33] Althaus D. Niedriggeschwindigkeitsprofile: Profilentwicklungen und Polarenmessungen im Laminarwindkanal des Instituts für Aerodynamik und Gasdynamik der Universität Stuttgart. Vieweg; 1996.
- [34] Ribnitzky D, Berger F, Petrovic V, Kuhn M. Hybrid-lambda: a low specific rating rotor concept for offshore wind turbines. In: Wind energy science; 2023. Preprint.
- [35] Escalera Mendoza AS, Mishra I, Griffith TD. An open-source NuMad model for the IEA 15 MW blade with baseline structural analysis. AIAA Paper 2023-2093. In: AIAA SciTech forum; 2023. <https://doi.org/10.2514/6.2023-2093>.